Microrobotic Control of Paramecium Cells using Galvanotaxis

Naoko Ogawa*, Hiromasa Oku*, Koichi Hashimoto†‡ and Masatoshi Ishikawa*
*Graduate School of Information Science and Technology, the University of Tokyo
7–3–1, Hongo, Bunkyo-ku, Tokyo 113–8656, Japan
†Graduate School of Information Sciences, Tohoku University
Aramaki Aza Aoba 01, Aoba-ku, Sendai-shi, Miyagi 980–8579, Japan
‡PRESTO, Japan Science and Technology Agency
4–1–8 Honcho Kawaguchi-shi, Saitama 332–0012, Japan
E-mail: {Naoko_Ogawa,Hiromasa_Oku,Masatoshi_Ishikawa}@ipc.i.u-tokyo.ac.jp, koichi@ic.is.tohoku.ac.jp

Abstract— **Our goal is to control microorganisms as micro-scale smart robots for various applications. In this paper, we introduce two approaches: a novel visual feedback control system for Paramecium cells and a dynamics model of Paramecium galvanotaxis (intrinsic reaction to electrical stimulus) for procise actuation. In the former part, we propose a microrobotic control system of cells using high-speed tracking. we have controlled Paramecium cells by utilizing the galvanotaxis. Experimental results for periodic zigzag motion and trapping within a small region 1 mm wide demonstrate the possibility of using microorganisms as micromachines. In the latter part, dynamics model of galvanotaxis. we construct a novel model of galvanotaxis as a minimal step to utilizing Paramecium cells as micro-robots. Bumerical experiments for our model demonstrate realistic behaviors, such as U-turn motions, like those of real cells.**

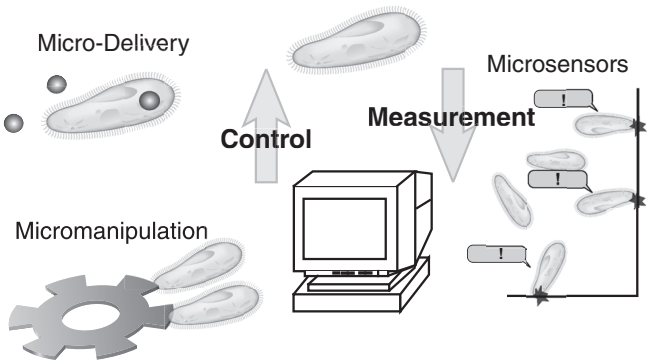

Fig. 1. The concept of our goal: to utilize microorganisms as smart micromachines.

I. Introduction

Recent progress in biotechnology has resulted in a growing interest in and increased demands for measurement and control of the micro- and nano-scale world. However, such measurement and control require human operators with high dexterity, expertise, and long experience. Hence, automation technologies to assist operators are needed. Yet, in conventional micromachine technology, there remain many problems to be solved before its practical application becomes realistic; these problems are mainly due to the still relatively young and undeveloped nature of the field and the limited technology available.

Our approach to overcome these problems is to utilize naturally occurring micromachines, or microorganisms. For all living things, detection of changes in the environment and quick reaction are essential for survival. Therefore, microorganisms have acquired sophisticated sensors and actuators through the course of their evolution. If we can develop techniques to control them freely, we can realize multi-purpose, programmable microrobotic systems superior to existing micromachine systems. Our goal is to eventually integrate controlled microorganisms and information processing systems, as illustrated in Fig. 1. By controlling microorganisms, we aim to achieve various applications, such as cell manipulation, microscopic delivery, smart microsensors, and assembly of micro-electro mechanical systems (MEMS).

Actuation of microorganisms is a key technology for realization of our goal. In particular, noncontact and non-invasive methods are desirable. One possible technique, which we focus on here, is to utilize "taxis" of microorganisms, an intrinsic locomotor response toward or away from an external stimulus. For example, many protozoa and bacteria exhibit a behavior called galvanotaxis, that is, taxis in response to an electrical stimulus. This implies that it is possible to control their motion by adjusting the electrical stimulus.

Although a number of studies on MEMS have been made [1], and many biosensors using microorganisms have been developed [2], there seem to be very few studies that have focused on microorganisms as smart motile machines, not just as tools. Arai manipulated yeast cells freely and dexterously by laser micromanipulation [3]. His concept differs from ours, however, in that the intrinsic nature of microbes was not utilized for actuation in his work. Fearing and Itoh are pioneers in using microorganisms as machines and they independently established a firm basis for this possibility [4], [5]. Now we would like to further improve their capabilities using a high-speed tracking system. As a first step, here we report on motion control of swimming

cells.

In this paper, we introduce two approaches for micro-robotic control of cells: synthetic and analytic. In the former part, we propose a novel system that can continuously control moving cells using a high-speed tracking system. This system was constructed for validating the feasibility of single-cell-level control. Experimental results demonstrate the capability of the system using *Paramecium caudatum* cells. In the latter part, we describe a dynamics model of Paramecium galvanotaxis for more precise control. Numerical experiments for our model demonstrate realistic behaviors, such as U-turn motions, like those of real cells. These works were also described in our publications [6], [7].

II. Tracking of Motile Cells

In this paper, we introduce a high-speed tracking system into the system for actuating cells. We describe the significance of the tracking technique and the system design.

A. Why Tracking?

To realize free and precise control of cells, some requirements for the observation are: (1) continuous observation of quickly swimming cells with no fixation, (2) a sufficiently large working area for free control, and (3) detailed observation of a specific cell with high magnification for precise actuation.

We found, however, that most conventional microscope systems, could not satisfy these demands: (1) Continuous observation was quite difficult, because cells swim very quickly. Instead, physical or physiological fixation had to be performed on the cells. (2) The working area was limited to inside of the visual field. (3) So as not to lose cells, we were compelled to observe them with low magnification, thus preventing detailed observation of the cell properties.

Especially, in most conventional micromanipulation systems, the working area is limited to within the small visual field of a microscope under high magnification, thus preventing completely free control. For example, Fearing controlled the trajectory of a *Paramecium caudatum* cell using galvanotaxis [4]. Itoh also controlled a *Paramecium caudatum* cell and actuated it to rotate a micro-impeller [5]. In their system, however, the working areas were limited to within their fixed visual fields. In order to realize more advanced actuation of microorganisms, this constraint must be eliminated.

To overcome these obstacles, we adopted a tracking method. In this paper, we mainly use the term "tracking" in the sense that the camera pursues a target so as to keep it always in the center of the visual field (sometimes we also call it "lock-on tracking"), while in general, the term "tracking" has a wider meaning, such as just locating the position of moving targets, or extracting targets from a background. As shown in Fig. 2, a lock-on mechanism can be realized by moving the position of the specimen on a stage so that the camera always keeps the target at the center. Although this can also be achieved by moving the camera and the microscope, we did not adopt this technique because it was much easier to move the stage.

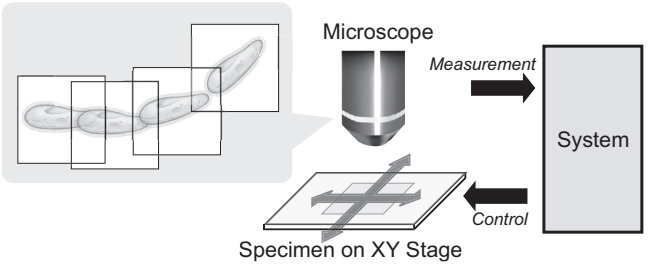

Fig. 2. Lock-on tracking scheme. The camera pursues a target so as to keep it always in the center of the visual field.

B. Previous Work on Tracking

Lock-on tracking of microorganisms is one of the key techniques that many biologists have sought for, because it allows the natural ecology of cells swimming freely *in vivo* to be continuously observed, without fixing them or slowing them down.

However, examples of lock-on tracking of cells in previous studies are extremely rare, whereas, we can find many works on cell tracking in a broad sense. For instance, Thar *et al.* tracked many microorganisms simultaneously with high spatial resolution by using laser beams and CCD cameras [8]. Strickler recorded trajectories of free-swimming copepods mating by using matched spatial filters [9]. Kuo *et al.* used scattered laser light to track and evaluate the activity of *Listeria* [10]. Teunis *et al.* located the three dimensional positions of the moving cilia of protozoa under a microscope [11]. Hasegawa *et al.* constructed a system to record the position of swimming microorganisms automatically [12]. Zimmer *et al.* tracked migrating cells individually using an active contour method [13]. Acton *et al.* detected the position and rotation of leukocytes [14]. These studies, although quite interesting, achieved merely simple positioning, locating, and recording of cells, without pursuing the cells and keeping them in the center of view. These systems allowed continuous observation, but not large workspaces and high magnification.

Berg *et al.* realized lock-on tracking by detecting the displacement of a target every 1/12 second using six optical fibers and photomultipliers, and automatically moving the chamber by mounting it on a stage [15]. His group succeeded in obtaining the three-dimensional trajectory of *Escherichia coli* [16], [17]. Enderlein adopted a similar method by moving the stage, but for tracking of fluorescent molecules, not for cells [18]. Though Berg's system had a remarkable recording ability, it was not suitable for real-time control applications, because it provided the information obtained only in an off-line manner, unlike our system, which allows us to acquire information in real-time.

Also, most tracking systems, including Berg's one, could detect only a few features of the target, such as its position.

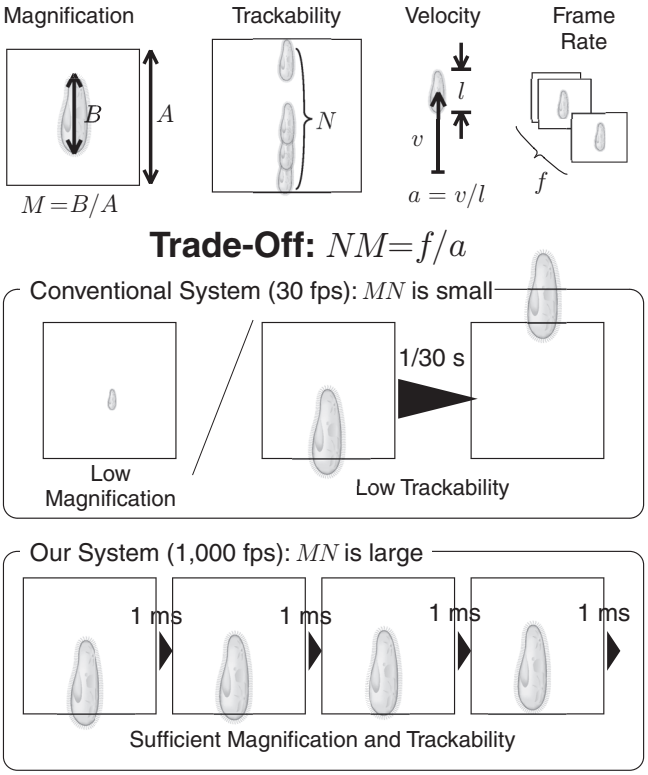

Fig. 3. Trade-off between magnification and trackability in microscopic tracking.

To identify a cell and execute intelligent tasks, various types of information about the cell are required. Moreover, each system was specially designed for a specific target, thus lacking versatility. As discussed later, our system has an advantage in that it is versatile and able to extract various features in real-time.

C. Necessity for High-Speed Vision

One major problem in tracking objects with a microscope is the trade-off relationship between magnification and trackability mentioned above; as the magnification increases, it becomes more difficult to track the target continuously. When the frame rate of the vision system is low, it is difficult to ensure both magnification and trackability.

As illustrated in Fig. 3, suppose that a target moves linearly with constant velocity (a times its diameter per second). Let M be the magnification index, i.e., the ratio of the target length to the visual field width ($M = 1$ means that the target fits exactly in the visual field), f the frame rate of the vision system, and N the trackability index, defined as the number of frames for the target to cross over the visual field. In other words, N represents a margin required in order not to lose the target, assuming that the camera stands still. It is desired that both the magnification index M and the trackability index N be large for detailed observation and quick control.

Now we derive the trade-off relationship. We introduce intermediate parameters: the diameter of the target l [m], its physical velocity v [m/s] ($a = v/l$), and the actual width of the visual field observed L [m] ($M = l/L$). Then the time t [s] needed for the target to cross over the visual field with the width L is calculated as:

$$t = L/v = 1/aM.$$

Because N is the number of frames for this process, we can express N as

$$N = tf = f/aM.$$

Thus the trade-off relationship can be written as

$$NM = f/a \qquad \text{(const.)}, \tag{1}$$

which is independent of the target size l. This implies that certain qualities for both magnification and trackability (i.e., sufficiently large M and N) is not ensured by an insufficient frame rate, when the target moves fast (i.e., a is large).

Most bacteria can swim as fast as 50 diameters/s [15] or 500 μm/s ; the frame rates required for these speeds are well beyond the normal video rate and must be analyzed differently, as pointed out in [19]. To be more precise, for conventional vision systems with a frame rate of around 30 Hz, we can estimate the value of NM to be 0.6, which is too small for our stated goal, namely ensuring sufficient magnification and trackability. For this reason, we need a vision system with a higher frame rate. As mentioned later, in this paper we used a high-speed vision system with a 1-kHz frame rate, so that NM can be over 20, which is enough for our purposes.

D. Visual Servoing for Real-Time Control

We need not only the observation of cells; our objective is to control moving cells using the information obtained. For the purpose of real-time control, the vision system must provide high-speed output of information, in addition to high-speed input of scenes. The system must extract information useful for control from the images in real-time. In other words, observation systems must be embedded in the high-speed servo loop for cell control.

III. Galvanotaxis Control System

A. Overall System Configuration

The configuration of the overall system and its block diagram are illustrated in Figs. 4 and 5, respectively. This system utilizes a microorganism tracking system [20].

An electrical stimulus is applied to cells swimming in a chamber on an electrical stimulus input device mounted on an XY stage. The stage is controlled by a high-speed vision system so as to keep a cell in the center of the field of view. By reading encoders on the stage and performing corrdinate transformation, we can obtain the global position of the cell. The orientation of the cell is also calculated from image features. Tracking is based on a dynamic image-based look-and-move structure [21].

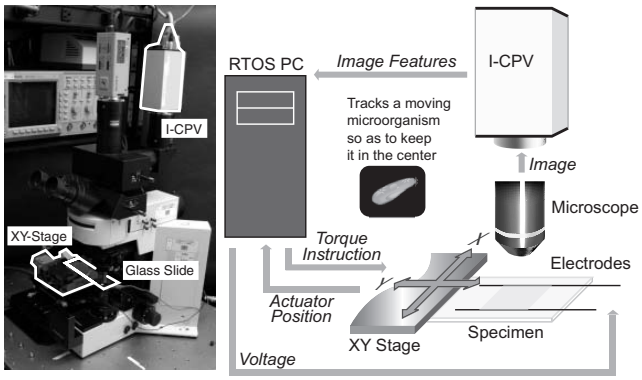

Fig. 4. System configuration.

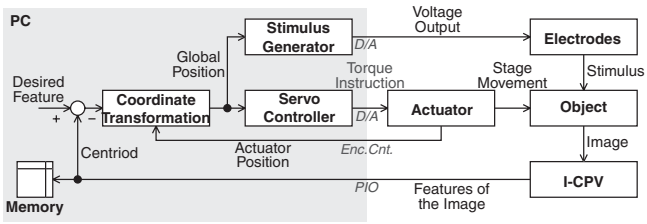

Fig. 5. Block diagram of the system.

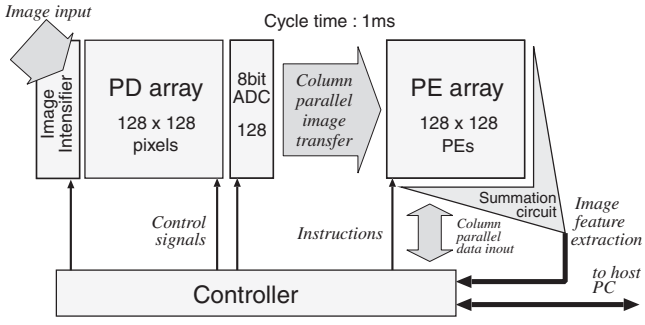

Fig. 6. Block diagram of I-CPV system.

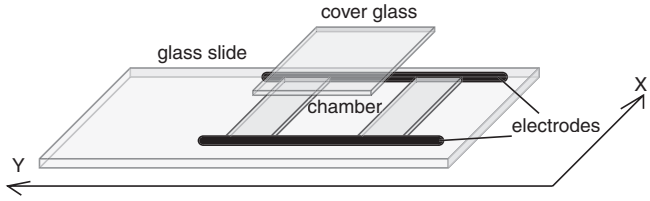

Fig. 7. Electrical stimulus input device.

B. Vision System

As discussed in II-C, a high frame rate is required for the vision system in order not to lose the target at high magnification. Moreover, an observing method with weak light, such as dark field microscopy, is needed so as to prevent heat and light influence on the cells.

To obtain dark images very quickly, we adopted a so-called I-CPV system jointly developed by Hamamatsu Photonics K.K. and one of the authors of the present paper (Ishikawa) [22]; this is a Column Parallel Vision (CPV) system with an image intensifier. CPV is a high-speed vision system developed for robotic applications [23].

A block diagram of the I-CPV is depicted in Fig 6. It captures and processes an 8-bit gray-scale image with 128×128 pixels and 1-kHz frame rate. I-CPV has a 128×128 photodetector (PD) array and the same number of programmable general-purpose processing elements (PEs). The captured image is amplified several thousand times by the image intensifier and transmitted by a CMOS sensor module (consisting of the PDs and A-D converters) to the PEs in a column-parallel manner. Each PE is based on the S^3PE architecture [24], which adopts a SIMD-type program control, and can process image data completely in parallel. Each PE is connected with a summation circuit, so that it can execute various processes, such as global image feature extraction, edge extraction, embossing and blurring, within 1 ms.

In the system proposed here, the I-CPV system is mounted on an upright optical microscope (Olympus, BX50WI) and captures dark-field images. The images are also captured by a CCD camera for convenience of monitoring. From the captured images, the I-CPV calculates image features and sends them to the PC. These features are used for the visual feedback control of an XY stage and microorganisms.

C. XY Stage

The PC controls the position of a chamber fixed on the XY stage by sending instructions to the stage. The XY stage (SMC, LAL00-X070) has two orthogonal axes, X and Y, whose stroke is 25 mm. Each axis has a linear coil actuator to control the stage position. It also has encoders with 1 μm precision on each axis. By controlling the stage according to the extracted target position, as described later, lock-on tracking of the target is achieved.

D. Electrical Stimulus Input Device

Fig. 7 shows the electrical stimulus input device. Two carbon electrodes of 0.5-mm diameter are placed in parallel on a glass slide, so that we can control the electrical stimulus in one direction perpendicular to the electrodes. The distance between them is 22 mm. Between the electrodes, there is a chamber 0.17 mm in depth to contain the specimen, The chamber constrains the motion of the cells within a two-dimensional plane. In order to maintain the chamber depth and to suppress evaporation of the medium, a cover glass is placed on the chamber.

The PC provides a voltage in the range ±10 V to the electrodes via a D/A converter board (Interface, PCI-3310). By feedback of the image feature values acquired by the I-CPV, it is possible to control the voltage in real-time according to the target status.

The whole system is controlled with a frequency of 1 kHz by the PC running a real-time OS (800 MHz, ART-Linux). During each cycle, the PC sets the electrical

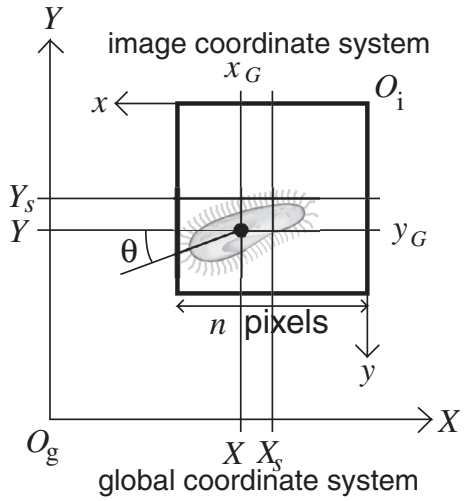

Fig. 8. Relationship between two coordinate systems.

stimulus applied to the microorganisms in the chamber, the I-CPV then captures the image of the target and calculates its feature values, and the PC sends instructions to the XY stage so as to track the target.

E. Tracking of Cells

As mentioned above, we adopted a tracking method called Microscopic Visual Feedback [20]. In our system, we extended it by adding a new feature for computing the target orientation to the version previously reported.

The I-CPV system provides the 0th, 1st and 2nd moments of the image every 1 ms [25]. As is well known, the centroid $(x_{\rm G}, y_{\rm G})$ of the target, and its tilt angle θ, shown in Fig. 8, are calculated using a given 0th moment m_0, 1st moments m_x and m_y, and 2nd moments m_{xx}, m_{yy} and m_{xy} (*e.g.*, see [26]):

$$x_{\rm G} = m_x/m_0, \quad y_{\rm G} = m_y/m_0, \tag{2}$$

$$\theta = \frac{1}{2}\arctan\left(\frac{2B}{A-C}\right), \tag{3}$$

where $A = m_{xx} - m_x^2/m_0$,
$B = m_{xy} - m_x m_y/m_0$,
$C = m_{yy} - m_y^2/m_0$.

The target point $(x_{\rm G}, y_{\rm G})$ is now expressed in the local, egocentric coordinate system. The PC restores the global, allocentric target position (X, Y) given by

$$\begin{pmatrix} X \\ Y \end{pmatrix} = -\frac{p}{m}\begin{pmatrix} x_{\rm G} - \frac{n}{2} \\ y_{\rm G} - \frac{n}{2} \end{pmatrix} + \begin{pmatrix} X_{\rm s} \\ Y_{\rm s} \end{pmatrix}, \tag{4}$$

where $(X_{\rm s}, Y_{\rm s})$ is the XY stage position sent from the encoders to the PC, p is the pixel pitch, n is the number of pixels along an edge of the visual field, and m is the magnification. The minus sign is due to the reversed visual field of the microscope image. Thus the trajectory and the orientation of the target are reconstructed.

The error values in displacement of the target are used to obtain the desired position of the XY stage. The servo system for the stage is designed by using the Smith-Davison design rule [27]. The controller compensates for friction and gravity. By controlling the XY stage, the target is always located in the center of the visual field. At this time, information about the target orientation θ is not used for tracking and control. However, these kinds of higher order information will be necessary for more precise control in the near future.

F. Segmentation and Matching

The tracking method introduced above does not work appropriately when there are two or more cells in the field of view. To solve this problem, segmentation of multiple cells and matching of the target between frames are realized by an algorithm called self-windowing [28], using some of the intrinsic characteristics of high-speed imaging, which are described below.

As the frame rate of the vision system becomes higher, the difference between frames decreases. In a vision system with sufficiently high frame rate, for example 1 kHz, we can say that the difference between a point in one frame and a corresponding point in the next frame is very small, at most one pixel. Thus an object in one frame will always be contained within a one-pixel dilation of the object itself in the next frame. In other words, we have only to pay attention to this dilated region for recognition of the target in the next frame, and can ignore the remaining region, including other objects and the background. This dilated region is used as a mask for cutting-out the target and for matching between frames. Of course, although this method cannot be applied when two objects are overlapped, the information about their orientation or velocity computed by I-CPV would be useful for distinguishing them.

G. Control of Cells

As illustrated in Fig. 5, the image features that are fed back are used for stimulation of the cell. When the PC receives feature values from the I-CPV, it adjusts the stimulus voltage applied to the electrodes.

For example, the system can reverse the voltage when a cell goes out of a certain region, as illustrated in Fig. 9. This allows us to trap the cell within the region. This trapping technique will be a powerful tool for advanced actuation in our future microsystems, such as standing-by before an operation or positioning of an object.

IV. Tracking Experiments

In this section, we will describe the experimental results to demonstrate the control capability of the proposed system using motile cells.

A. Materials

Paramecium caudatum, a kind of protozoa, was used in our motile cell control experiments. It is a kind of

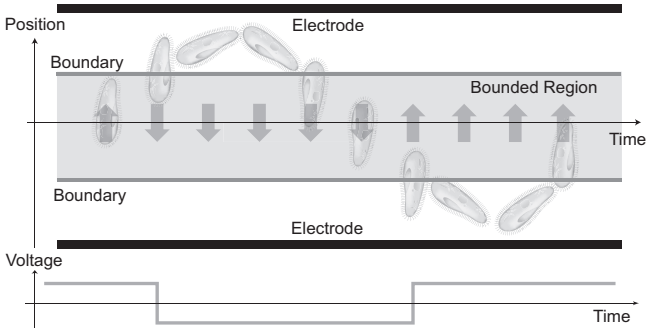

Fig. 9. Trapping of a microorganism within a region.

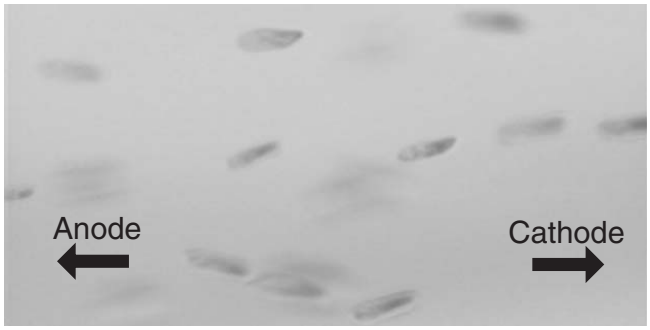

Fig. 10. Galvanotaxis of *Paramecium caudatum*. They swim toward the cathode.

unicellular protozoa with an ellipsoidal shape, inhabiting freshwater. The size of a cell is about 200 μm in length, large enough to be observed easily by an optical microscope. *Paramecium* has very strong galvanotaxis [29]; when the electric field is applied, it tends to swim toward the cathode, as shown in Fig. 10. We can say that their motion toward the cathode is not caused by electroosmosis or other non-biological phenomena, because we confirmed that dead cells do not move in the presence of the electric field. It is a byproduct of the electrophysiological nature of the cell. The ciliary motion of *Paramecium* is determined by the membrane potential and the accompanying changes in ion concentration in the cell. When an external electrical stimulus is applied, it modifies the membrane potential and alters the ciliary movements, consequently exerting an influence on the cell motion. Strong galvanotaxis of *Paramecium* makes it suitable for external control.

Wild-type *Paramecium* cells were cultured at 20-25°C in a soy flour solution. Cells grown to the logarithmic or stationary phase (4-10 days after incubation) were collected together with the solution, filtered through a nylon mesh to remove debris, and infused into the chamber.

B. Open-Loop Control Experiment

First, open-loop control of cells was performed. Cells were controlled by a time-varying stimulus whose pattern was fixed in advance. The electrical stimulus was applied in the X direction, and reversed every 6 s. The strength of the voltage gradient was 4.1 V/cm (9 V across a 22 mm gap). A 20× objective lens was used for magnification.

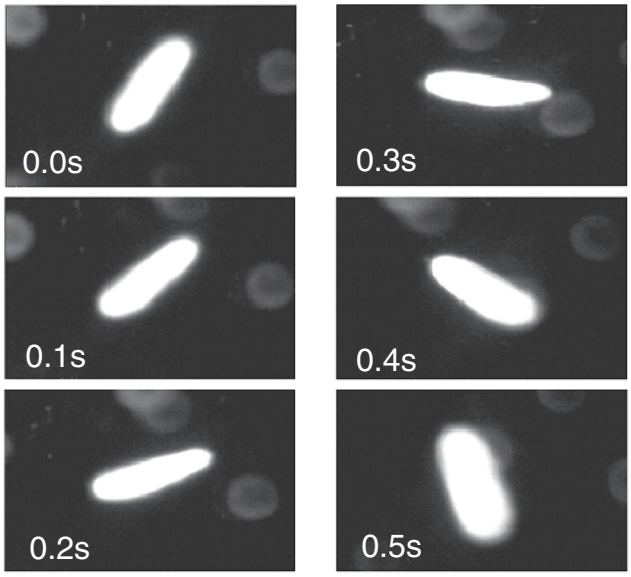

Fig. 11. Sequential photographs of a cell making a U-turn by stimulus reversal (0.1-s intervals).

Fig. 11 shows some sequential photographs of a cell making a U-turn by stimulus reversal, as captured by the CCD monitoring camera. The time interval between each image is 0.1 s. The cell motion was affected by the stimulus and the cell position was always kept in the center of the image field.

Fig. 12 shows the time sequence of the positions parallel (X) and perpendicular (Y) to the electric field, respectively. Arrows indicate the direction of the electric field. For the X direction, the cells reacted sensitively to the stimulus and showed almost uniform motion, whereas the motion for the Y direction seemed almost independent of the stimulus. Small fluctuations in Y position were observed, which were due to the spiral wriggling movement of the cells.

As discussed in III-E, we can reconstruct the trajectory and the orientation of the target from the features extracted by the I-CPV system. Fig. 13 shows the trajectory of cell #3 presented in Fig. 12, and its orientation (small arrows), where the direction of the electric field is horizontal. The spiral path and the ever-changing orientation of the cell were reconstructed with high fidelity. It also indicates that both high magnification and good trackability over a large working area were achieved.

C. Closed-Loop Control Experiment

In order to confirm the ability of closed-loop visual feedback control of cells, we performed a simple trapping experiment, as described in III-G; the stimulus was adjusted in real time according to the target status. The width of the trapping region was set to 1 mm. The voltage was reversed when the cell moved out of the boundaries. Other conditions were the same as those of the open-loop control experiment described above.

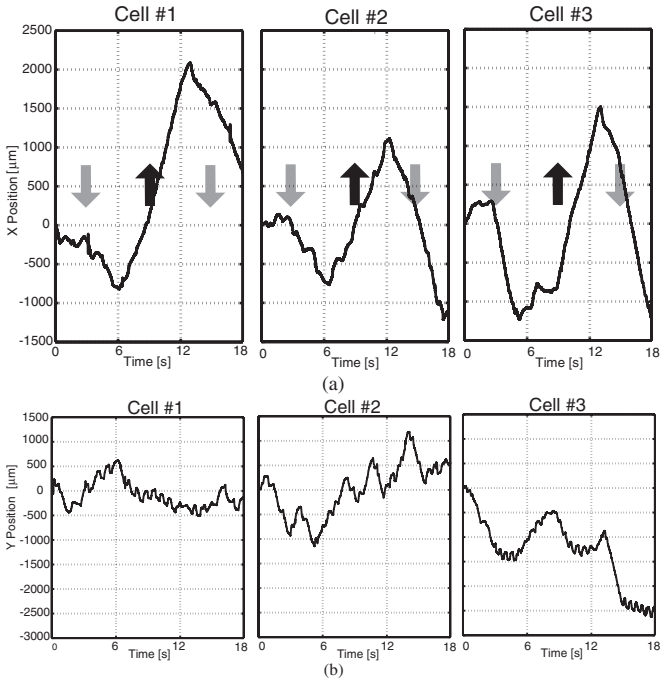

Fig. 12. (a) X position (parallel to the electric field) of cells in the open-loop control experiment. Arrows indicate the direction of the applied electric field. (b) Y position (perpendicular to the electric field) of cells in the open-loop control experiment.

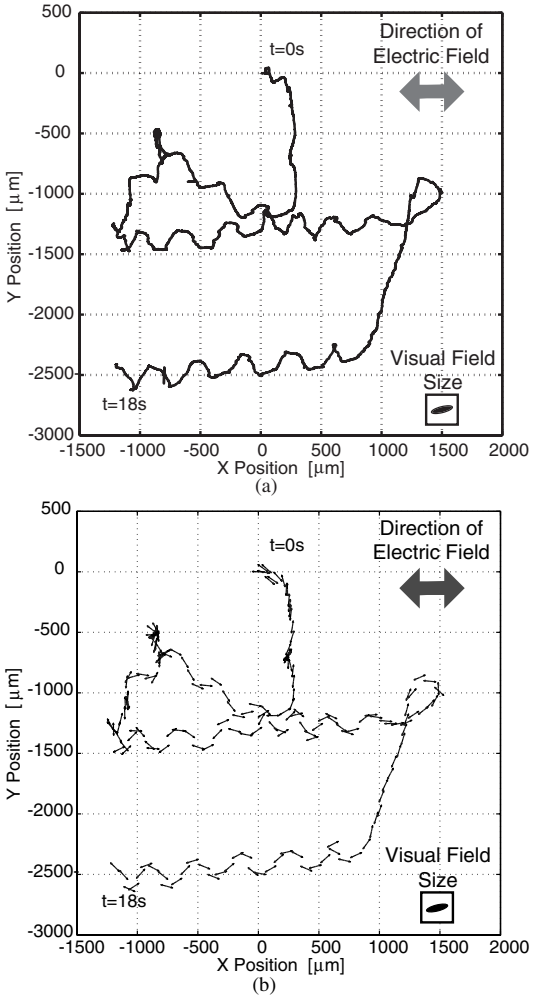

Fig. 13. (a) Trajectory of a cell in the open-loop control experiment. (b) Orientation of a cell (small arrows) in the open-loop control experiment.

Fig. 14 and Fig. 15 demonstrate results of the control experiment. Fig. 14 shows the time sequence of both the voltage and the position parallel to the field (X), and the position perpendicular to the field (Y). The voltage was reversed when the cell went out the region. Consequently the cell swam back and forth in the region. The trajectory of the cell is shown in Fig. 15.

These results indicate that we achieved continuous open-loop and closed-loop control of galvanotaxis of motile cells by target tracking. It is a first step for realizing microrobotic system composed of microorganisms.

V. Model of Galvanotaxis

A. Dynamics Model as a Robotic Scheme

As mentioned in the former part of this article, we achieved a simple motion control of Paramecium cells, as well as other recent studies did [4–6]. However, these studies were based on simple empirical rules without knowledge about the physical properties of the cells, and thus had limited control performance. For instance, when a stimulus was toggled to turn a cell, there was a considerable time lag of several hundred milliseconds between the start of the stimulus and completion of the turn, causing the cell to turn too far [5], [6].

To realize more precise control, it is essential to deal with Paramecium in the framework of standard robotics, that is, to discuss its dynamics, trajectory planning, advanced motion control and so on. The minimal and most basic preparation required for this discussion is a mathematical and quantitative model of the physical dynamics of Paramecium.

Unfortunately, there seem to be no studies on modeling of Paramecium galvanotaxis from such a robotic point of view. Conventional Paramecium models have mainly been physiological and biochemical ones that have focused on its membrane potential or signal transduction, ignoring its physical properties. A very rare physical model proposed by Naitoh *et al.* considered only the behavior with no electrical stimulus [30]. Although Sakane *et al.* and Hirano *et al.* constructed models for chemotaxis and the response called avoiding reaction [31], [32], they are not applicable to galvanotaxis, which has a fundamentally different mechanism from other taxis or reactions. Fearing and Itoh independently performed pioneering experiments on controlling protozoa, but their approach was based on empirical rules [4], [5].

Conventional biology has provided only qualitative explanations for galvanotaxis at the physical level [29], [33]. However, practical application of galvanotaxis requires its

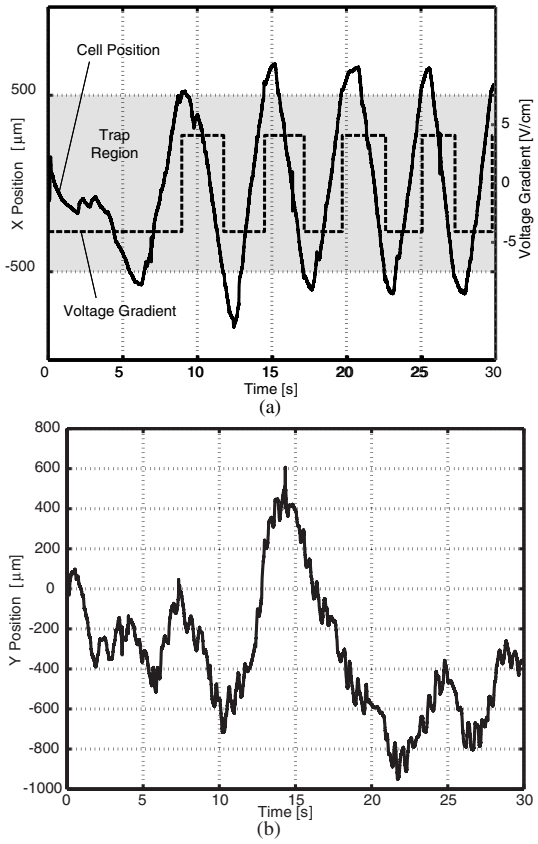

Fig. 14. (a) Applied voltage (dashed line) and X position (parallel to the electric field) of a cell (solid line) in the closed-loop control experiment. The shaded region is the bounded region for trapping. (b) Y position (perpendicular to the electric field) of a cell in the closed-loop control experiment.

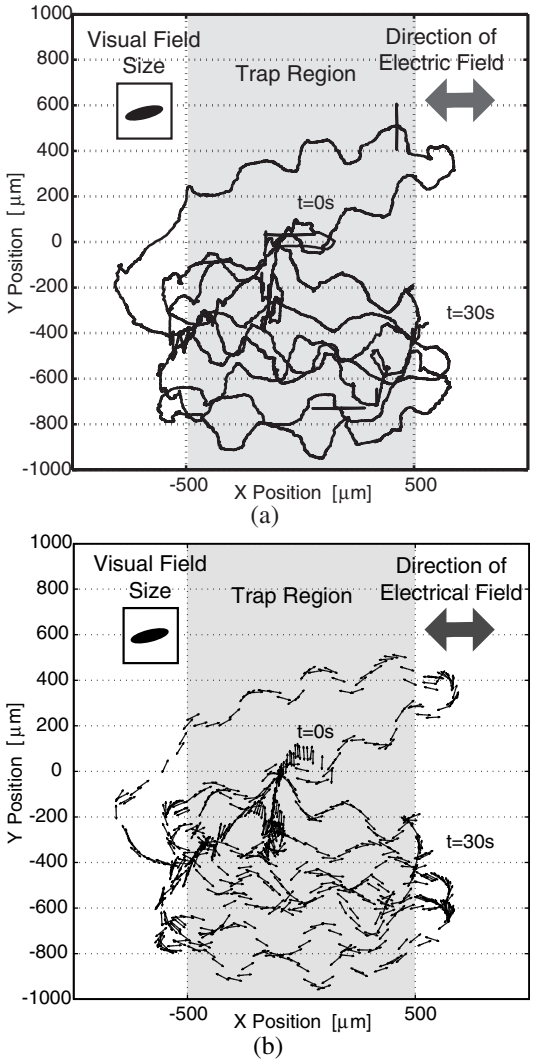

Fig. 15. (a) Trajectory of a cell in the closed-loop control experiment. (b) Orientation of a cell in theclosed-loop control experiment (small arrows). The shaded region is the bounded region for trapping.

quantitative evaluation. Robotic treatment of cells will not become feasible without a mathematical description of single cell motion.

As a minimal preparation for a microrobotic approach to Paramecium control, this paper describes a dynamics model of Paramecium galvanotaxis.

B. Paramecium and Its Galvanotaxis

1) Mechanism of Paramecium Galvanotaxis: A paramecium cell in an electric field shows characteristic ciliary movement. Assume an imaginary plane that is perpendicular to the electric field and located near the center of the cell somewhat close to the cathodal end, dividing the cell into two parts, as illustrated in Fig. 16. By applying the electric field, cilia on the anodal end begin to beat more frequently (ciliary augmentation), and beating on the cathodal end becomes reversed and more frequent (ciliary reversal). This is called the Ludloff phenomenon [34], and it provides a qualitative explanation for galvanotaxis: the asymmetry in direction of the ciliary beatings on the hatched region shown in Fig. 16 generates a rotational force and orients the cell toward the cathode (ciliary motions away from this region are symmetrical and do not contribute to the rotation).

The cause of galvanotaxis can be understood to be a combination of electrochemical, physiological and physical factors. While electrochemical and physiological factors are not so dominant for control performance, physical factors play an important role in control of cells. Therefore, this paper concentrates on physical factors, while regarding electrochemical and physiological ones as black boxes.

C. Assumptions

1) Simplification of Cell Motion: Strictly speaking, the motion of a Paramecium cell is composed of (1) forward propulsion, (2) a rotation around its longitudinal axis, and (3) a rotation around its dorsoventral axis due to its asymmetrical shape. Consequently, the cell swims forward spinning along a spiral [30]. The most dominant element in galvanotaxis is element (1). For simplicity, we will not discuss the other two elements, which are not essential for

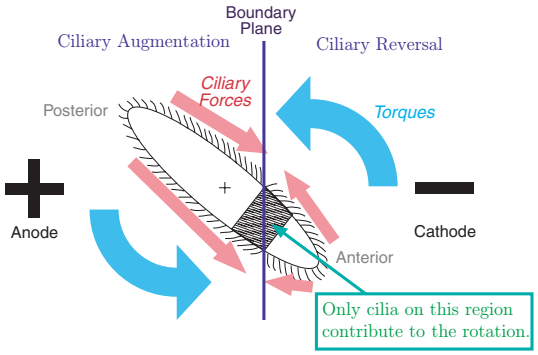

Fig. 16. Qualitative explanation for galvanotaxis.

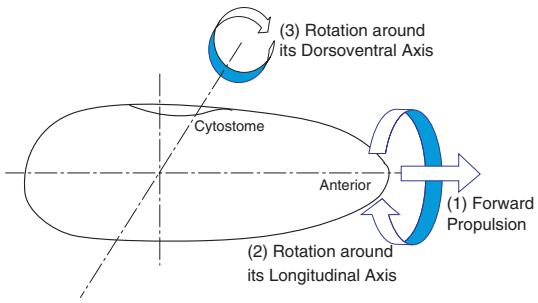

Fig. 17. Schematic representation of forces produced by movements of cilia. Reproduced from reference [30] with modification.

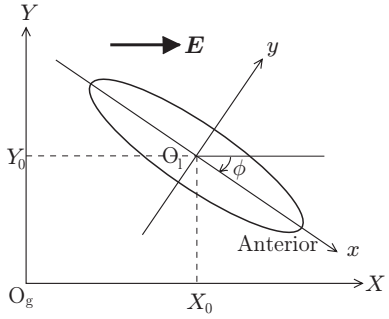

Fig. 18. Relation between the global coordinate system (X, Y) and the local coordinate system (x, y).

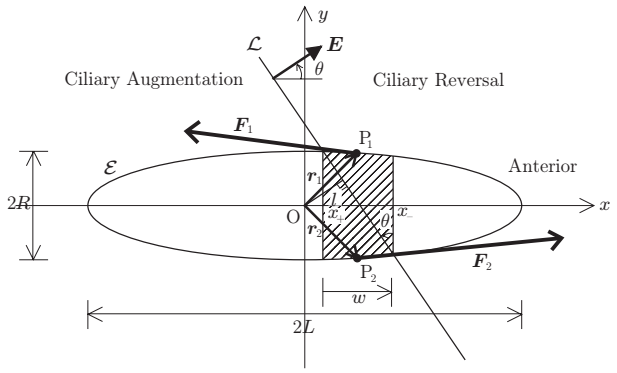

Fig. 19. Parameters in the local coordinate system.

galvanotaxis. This assumption means that the cell just goes straight when there is no electric field.

By disregarding the rotation components, we can describe the cell motion in a two-dimensional plane including the cell axis and the electric field vector. Hereafter we consider cell motion only in this plane. At the same time, because motions of the cilia can be assumed to be symmetric with respect to the plane, the movements of the cilia on the plane can sufficiently represent the movements of all cilia. Thus, we consider the cell as a two-dimensional ellipsoid on the plane.

2) Assumptions on Ciliary Motion: We assume that cilia are distributed uniformly on the edge of the ellipsoid with linear density n. For simplicity, we consider only two states for beating, reverse and normal. The cilia are oriented towards the anterior side in reverse beating, and towards the posterior side in normal beating. In the presence of an electric field, imagine a plane perpendicular to the field (hereinafter referred to as "a boundary plane"). This plane divides the cell into two regions; cilia are considered to be normal in the anodal side, and reversed in the cathodal side. The boundary plane is formed in the cathodal side, and the shortest distance between the plane and the center of the cell is l.

The beating frequency is assumed to be uniform over the whole cell, with a value φ_0 in the absence of an electric field (hereinafter referred to as "regular state"). When an electric field E is applied, the frequency increases to $\varphi = (1+\beta E)\varphi_0$ ($\beta > 0$). Let f_0 be a propulsion force yielded by one cilium in the regular state, the force being proportional to the frequency φ_0 ($f_0 = \alpha\varphi_0$). Let $f = \alpha\varphi = (1+\beta E)f_0$ be the force in the presence of the electric field.

3) Coordinate Systems: We define two coordinate systems, a global one (X, Y) and a local one (x, y), on the plane, as shown in Fig. 18. The global coordinate system is allocentric, that is, fixed with respect to the external world, with the X-axis parallel to E. The local coordinate system (introduced to simplify the description) is egocentric, that is, fixed with respect to the cell, with the X-axis parallel to the longitudinal axis of the cell. Let ϕ be the angle of the cell axis in the global coordinate system ($\phi < 0$ in Fig. 18, for the sake of convenience in deriving the model).

Let the cell shape be an ellipsoid with a major axis $2L$ and a minor axis $2R$ ($L > R$). In the local coordinate system, the cell is represented as an ellipsoid $\mathcal{E}$:

$$\mathcal{E} : \frac{x^2}{L^2} + \frac{y^2}{R^2} = 1. \tag{5}$$

D. Model of the Torque

The phenomenon whereby a Paramecium cell swims toward the cathode is due to a torque caused by assymmetry of ciliary motion. In this section, we estimate this torque. First, consider an ellipsoid $\mathcal{E}$, as illustrated in Fig. 19.

For convenience, let us introduce $\theta = -\phi$, as the angle of the electric field in the local coordinate system. Then the

boundary plane is expressed as a line $\mathcal{L}$:

$$\mathcal{L} : y = -\frac{1}{\tan\theta}x + \frac{l}{\sin\theta}. \tag{6}$$

As mentioned in the former section, assymmetry of ciliary beating exists only at the substantially trapezoidal region formed by the intersection of the boundary plane and the ellipsoid (shown as hatched regions in Fig. 16 and Fig. 19). The forces excerted by cilia outside this region are symmetrical and do not contribute to rotation. Thus, we consider only the forces generated at this trapezoidal region.

The x positions of two lines that consist of the "upper" side and "lower" side of the trapezoid are equal to those of two intersecting points of $\mathcal{E}$ and $\mathcal{L}$. These two positions, x_- and x_+, are obtained as two roots of equation

$$\begin{aligned}(R^2\sin^2\theta + L^2\cos^2\theta)x^2 - 2lL^2\cos\theta \cdot x \\ + l^2L^2 - R^2L^2\sin^2\theta = 0,\end{aligned} \tag{7}$$

which is derived by eliminating y from Eq. (5) and Eq. (6) (this equation always has two real roots). Between these two intersecting points of $\mathcal{E}$ and $\mathcal{L}$, let x_+ be a point with larger y position, and x_- be a point with smaller y position.

Because it would be too complicated to consider all minuscule forces generated by each cilium, here we focus on the resultant forces for simplicity. We set the sites of action, $\mathrm{P}_1(x_\mathrm{a}, y_\mathrm{a})$ and $\mathrm{P}_2(x_\mathrm{a}, -y_\mathrm{a})$ ($y_\mathrm{a} \geq 0$), on the midpoints of the "height" of the trapezoid, and assume the directions of the forces to be tangential to the ellipsoid. Let us define the disposition vectors, $\boldsymbol{r_1} = \overrightarrow{\mathrm{OP}_1}$ and $\boldsymbol{r_2} = \overrightarrow{\mathrm{OP}_2}$.

Then we obtain

$$x_\mathrm{a} = \frac{x_- + x_+}{2} = \frac{lL^2\cos\theta}{R^2\sin^2\theta + L^2\cos^2\theta}. \tag{8}$$

Also, y_a is obtained by substituting Eq. (8) into Eq. (5):

$$y_\mathrm{a} = \frac{R}{L}\sqrt{L^2 - x_\mathrm{a}^2}.$$

The two tangential lines on the sites of action $(x_\mathrm{a}, \pm y_\mathrm{a})$ are given by

$$\frac{x_\mathrm{a}}{L^2}x \pm \frac{y_\mathrm{a}}{R^2}y = 1,$$

from which we get the inclinations of the two tangential lines,

$$m = \mp\frac{R^2 x_\mathrm{a}}{L^2 y_\mathrm{a}},$$

and we get normalized tangent vectors

$$\left(\frac{1}{\sqrt{1+m^2}}, \frac{m}{\sqrt{1+m^2}}\right).$$

Let $\boldsymbol{m}_1$ be the tangent vector at P_1, and $\boldsymbol{m}_2$ be that at P_2. Then unit force vectors, $\boldsymbol{e}_1$ at P_1 and $\boldsymbol{e}_2$ at P_2, are:

$$\begin{aligned}\boldsymbol{e}_1 &= -\boldsymbol{m}_1 \quad \text{(reverse beating)},\\ \boldsymbol{e}_2 &= \boldsymbol{m}_2 \quad \text{(normal beating)},\end{aligned}$$

considering the directions of ciliary beatings.

Moreover, let us suppose that the magnitude of the resultant force is proportional to the number of cilia n, and that n is proportional to the "height" of the trapezoid:

$$w = x_- - x_+,$$

which is a signed value whose sign is the same as θ. Then the propelling forces $\boldsymbol{F}_1$ and $\boldsymbol{F}_2$ at the points P_1 and P_2 respectively, are written as

$$\boldsymbol{F}_1 = fwn\boldsymbol{e}_1, \quad \boldsymbol{F}_2 = fwn\boldsymbol{e}_2.$$

By assuming that the center of gravity of the cell is located at the center of the ellipsoid, we find the torques at the points P_1 and P_2:

$$\boldsymbol{\tau}_1 = \boldsymbol{r}_1 \times \boldsymbol{F}_1, \quad \boldsymbol{\tau}_2 = \boldsymbol{r}_2 \times \boldsymbol{F}_2,$$

where one should note that these vectors are treated as three dimensional in calculating cross products.

Finally the torque rotating the cell body is given by:

$$\boldsymbol{\tau} = \boldsymbol{\tau}_1 + \boldsymbol{\tau}_2.$$

Since its x and y components are obviously zero, hereafter we call its z component, τ_z, the "torque".

Finally, by substituting $\phi = -\theta$, the torque is described in the global coordinate system as:

$$\begin{aligned}&\tau_z(\phi)\\ &= -\frac{4LR^2fns\sqrt{L^2c^2 + R^2s^2 - l^2}}{\sqrt{L^4c^4 + 2L^2R^2c^2s^2 + R^4s^4 - L^2l^2c^2 + R^2l^2c^2}},\end{aligned} \tag{9}$$

where $\quad s = \sin\phi, c = \cos\phi.$

This equation provides the torque generated in the Paramecium cell with the angle ϕ.

E. Dynamic Equation of Paramecium Cell

Using the torque estimated in previous section, we now discuss the motion equation of a Paramecium cell.

1) Dynamic Equation for Translational Motion: In the micrometer-scale world the Paramecium cells inhabit, the inertial resistance of the fluid is small enough to be negligible, and the viscous resistance becomes dominant instead. Hence we can apply Stokes' law, derived from the Navier-Stokes equation by ignoring inertial force.

Since the rigorous evaluation of viscous resistance around an ellipsoid is quite complicated, here we approximate the viscosity roughly by applying the formula for a sphere as a substitute. According to Stokes' law, the force exerted on a sphere with radius a, moving with velocity v in a viscous fluid is given by

$$F_\mathrm{s} = 6\pi\mu av, \tag{10}$$

where μ is the viscosity of the fluid. From this equation, the viscous force around the ellipsoidal cell can be obtained by replacing the radius a by the cell radius R. Thus the

motion equation for the translational motion of the cell can be roughly approximated by:

$$M\ddot{\boldsymbol{X}} + D\dot{\boldsymbol{X}} = \boldsymbol{F}, \tag{11}$$

where $\boldsymbol{X} = (X, Y)^{\mathrm{t}}$ is the cell position, $\boldsymbol{F} = 2fn|x_a|\boldsymbol{e}_{\boldsymbol{X}}$ is a forward propulsive force, $\boldsymbol{e}_{\boldsymbol{X}} = \frac{\boldsymbol{X}}{|\boldsymbol{X}|} = (\cos\phi, \sin\phi)^{\mathrm{t}}$ is a unit vector along the body axis, $D = 6\pi\mu R$ is the viscous friction coefficient, $M = \rho V$ is the cell mass, ρ is the cell density, and $V = 4\pi LR^2/3$ is the cell volume.

2) Dynamic Equation for Rotational Motion: We now derive a motion equation for rotational motion. As mentioned above, because evaluation of the viscosity around the ellipsoid is complicated, we again substitute Stokes' law for a sphere. A viscous resistance torque against the rotation can be approximated by assuming two mass points on the body axis at a quarter of the length $(L/2)$ from the origin, substituting $v = \dot{\phi} \cdot L/2$ and $a = L/2$ into the Stokes' law equation (10), and multiplying both sides by $L/2$:

$$\tau_{\mathrm{s}} = F_{\mathrm{s}}\frac{L}{2} = 6\pi\mu\frac{L}{2}\dot{\phi}\frac{L}{2}\frac{L}{2} = \frac{3}{2}\pi\mu L^3\dot{\phi}.$$

This derivation would be too rough and the coefficient $3/2$ might be unreliable; there could be a model error of several fold. Let us introduce δ to replace the coefficient and absorb the error. Thus, the motion equation for rotational motion is given by

$$I\ddot{\phi} + D'\dot{\phi} = \tau(\phi), \tag{12}$$

where $I = \pi M(R^2 + L^2)/5$ is the moment of inertia for an ellipsoid, and $D' = \delta\pi\mu L^3$ is the viscous friction coefficient.

3) Integration of Motion Equations: Integration of the motion equations for translational motion (11) and rotational motion (12) leads to the following equations:

$$\dot{\boldsymbol{y}} = A\boldsymbol{y} + \boldsymbol{B}(\boldsymbol{y}), \tag{13}$$

$$A = \begin{pmatrix} 0 & 0 & 1 & 0 & 0 & 0 \\ 0 & 0 & 0 & 1 & 0 & 0 \\ 0 & 0 & -D/M & 0 & 0 & 0 \\ 0 & 0 & 0 & -D/M & 0 & 0 \\ 0 & 0 & 0 & 0 & 0 & 1 \\ 0 & 0 & 0 & 0 & 0 & -D'/I \end{pmatrix},$$

$$\boldsymbol{B}(\boldsymbol{y}) = \left(0, 0, \frac{P}{M}\cos\phi, \frac{P}{M}\sin\phi, 0, \frac{\tau_z(\phi)}{I}\right)^{\mathrm{t}},$$

and where $P = 2fn|x_a|$ and $\boldsymbol{y} = (X, Y, \dot{X}, \dot{Y}, \phi, \dot{\phi})^{\mathrm{t}}$.

VI. Numerical Experiments and Comparison to Actual Data

We performed some numerical experiments to verify the motion equation (13) by using numerical analysis software (MATLAB, MathWorks Inc.).

TABLE I

Parameters of the proposed model.

Parameters	Values	Comments
Major cell axis $2L$	$100\,\mu$m	our strain
Minor cell axis $2R$	$25\,\mu$m	our strain
Boundary plane offset l	$10\,\mu$m	Reference [33], [35]
Viscosity of water μ	1.00×10^{-3} kg/(ms)	at 20 ℃
Cell density ρ	$1,000$ kg/m^3	same as water
Increase in beating freq. β	2.00×10^{-3} V^{-1}	

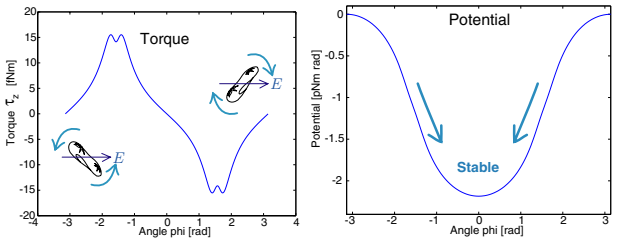

Fig. 20. Torque $\tau_z(\phi)$ generated by ciliary force (left) and its potential energy (right).

A. Preparation of Parameters

Table I shows several physical parameters used in the experiments. We obtained the cell size by observing cells incubated in our laboratory; the size we observed was smaller than the average [33]. The boundary plane offset l is estimated from several figures shown in previous studies [33], [35], for it is difficult to observe with our equipment. As for β, the increase in beating frequency with electric field, the value was estimated from the fact that the frequency almost doubled to around 50 Hz under a stimulation of around a few volts per centimeter, while that in the regular state was around 15-20 Hz [30].

The force yielded by cilia on unit length, f_0n, is still an unknown parameter. We estimated the order of f_0n by using the actual value of swimming velocity measured in past experiments.

The terminal velocity of a cell in the regular state was obtained by substituting $\ddot{\boldsymbol{X}} = \boldsymbol{0}$ into eq. (11) under conditions $E = 0$ and $\phi = 0$:

$$\dot{\boldsymbol{X}} = \boldsymbol{F}/D = \frac{|x_a|_{\phi=0}\boldsymbol{e}_{\boldsymbol{X}}}{3\pi\mu R}f_0n.$$

Since x_a equals to l at $E = 0$, we can estimate f_0n by:

$$f_0n = \frac{3\pi\mu R}{l}|\dot{\boldsymbol{X}}|. \tag{14}$$

According to our measurement of the cell velocity by using a high-speed vision system [36], their velocity is around $400\,\mu$m/s. Using this, we estimated f_0n to be 4.71×10^{-6} N/m.

B. Torque Profile $\tau_z(\phi)$

The left side of Fig. 20 shows the torque $\tau_z(\phi)$ as a function of ϕ. The torque affects the cell so as to decrease ϕ, that is, to make the cell turn toward the cathode.

C. Angular Stability in the Proposed Model

Equations (11) and (12) indicate that the motion equation of a Paramecium cell has nonlinearity that might make the model unstable. However, when the angle ϕ is sufficiently small, that is, the direction of the cell is close to that of the electric field, it is possible to make the model linear approximately. In this section, we will linearize the model to observe the stability for small ϕ.

In Fig. 20, the z component of the torque, $\tau_z(\phi)$, exhibits a gradual monotonic decrease near $\phi = 0$, which implies that it can be regarded as linear with respect to ϕ in this area. Therefore, $\tau_z(\phi)$ can be approximated using the inclination of the tangential line at $\phi = 0$:

$$\tau_z(\phi) \simeq \left.\frac{\mathrm{d}\tau_z}{\mathrm{d}\phi}\right|_{\phi=0} \cdot \phi = -4\frac{R^2 L f n\sqrt{L^2 - l^2}}{\sqrt{L^4 - L^2 l^2 + R^2 l^2}}\phi.$$

Then eq. (12) becomes:

$$\ddot{\phi} = -\frac{D'}{I}\dot{\phi} + \frac{Q}{I}\phi, \quad \text{where} \quad Q = -4\frac{R^2 L f n\sqrt{L^2 - l^2}}{\sqrt{L^4 - L^2 l^2 + R^2 l^2}}.$$

By defining a state variable $\tilde{\boldsymbol{y}} = (\phi, \dot{\phi})^{\mathrm{t}}$, the model of the cell rotation becomes linear around the origin:

$$\dot{\tilde{\boldsymbol{y}}} = \tilde{A}\tilde{\boldsymbol{y}}, \quad \tilde{A} = \begin{pmatrix} 0 & 1 \\ Q/I & -D'/I \end{pmatrix}.$$

The eigenvalues of this matrix $\tilde{A}$ are $\left(-D' \pm \sqrt{D'^2 - 4IQ}\right)/2I$, which are negative. Therefore, the cell is stable for small ϕ and its direction converges to $\phi = 0$.

In addition, the global stability was verified qualitatively by calculating a potential energy U for rotation. We defined U as $\tau_z = -\frac{\partial U}{\partial \phi}$ and computed it by numerical integration of eq. (9) with respect to ϕ. The right side of Fig. 20 shows the profile of U, indicating that the cell tends to approach $\phi = 0$ for all ϕ.

D. Simulation and Comparison of U-turn Motions

We have accumulated a large amount of data for Paramecium motion using a high-speed vision system called I-CPV (Fig. 21 A) [22] and a galvanotaxis continuous observation system (Fig. 21 B) [37]. Using these data, we adjusted the parameter δ to be 7.5, and verified the validity of the model.

When an electric field is applied in the direction opposite to the swimming direction of a cell, the cell makes a U-turn motion (Fig. 21 C). We tested whether our proposed model can demonstrate this phenomenon.

First, swimming trajectories for cells with eleven different initial orientations were calculated. Figure 21 D demonstrates all trajectories simultaneously. The cells were configured to all have the same initial position, namely, on the origin $(0, 0)$, but not their initial angles, which differed by intervals of 30°($-150°$, $-120°$, …, 150°). A 5.0-V/cm electric field was applied along the X-axis. The trajectory of each cell was calculated using an ordinary differential equation solver. As shown in Fig. 21 D, all cells starting from the origin turned toward the cathode, like the real ones.

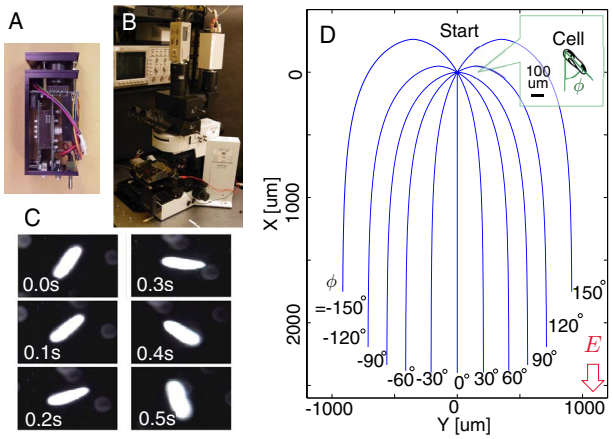

Fig. 21. A: High-speed vision system (I-CPV) [22]. B: Galvanotaxis continuous observation system [37]. C: U-turn motion observed by our system [37]. D: Demonstration of U-turn motions of cells.

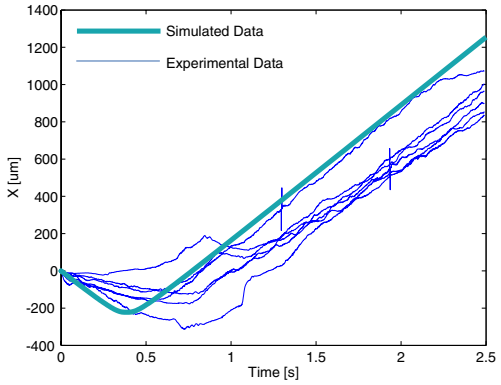

Fig. 22. Comparison between simulated data (thick line) and experimental data (thin lines).

Next, we compared simulated and experimental positions as shown in Fig. 22. We extracted positions along the electric field (X direction), because X-position is almost independent of fluctuations caused by spiral motions, which we disregarded.

Experimental data (thin lines) were obtained by high-speed measurement of the responses of a single cell for several levels of input electric field, using the galvanotaxis continuous measurement system [37]. The electric field applied to the cell had a step-like form, rising to 4.1 V/cm, and its position and angle were continuously measured at a 1-kHz frame rate by high-speed tracking using the I-CPV system [22], [36]. In Fig. 22, data for three seconds from the stimulus change in six trials are overlaid. Simulated data (thick line) was calculated under the conditions that the initial angle was the average of angles obtained from previously measured data. The simulated data was approximately in agreement with the experimental results.

VII. SUMMARY

In this paper, we introduce two approaches for micro-robotic control of cells. First, we proposed a novel system that can continuously control moving cells using a high-speed tracking system. Second, proposed a physical model of Paramecium galvanotaxis as the first step for micro-robotic application of microorganisms, and investigated its behavior by numerical calculations and experiments.

REFERENCES

[1] R. S. Muller, "MEMS: Quo Vadis in Century XXI?" *Microelectronic Engineering*, vol. 53, pp. 47–54, 2000.

[2] S. Daunert, G. Barrett, J. S. Feliciano, R. S. Shetty, S. Shrestha, and W. Smith-Spencer, "Genetically engineered whole-cell sensing systems: Coupling biological recognition with reporter genes," *Chemical Reviews*, vol. 100, no. 7, pp. 2705–2738, Jun. 2000.

[3] F. Arai, "Synchronized laser micromanipulation by high speed laser scanning—dancing yeasts—," in *Video Proc. 2003 IEEE Int. Conf. Robotics & Automation (ICRA2003)*, Sep. 2003.

[4] R. S. Fearing, "Control of a micro-organism as a prototype micro-robot," in *2nd Int. Symp. Micromachines and Human Sciences*, Oct. 1991.

[5] A. Itoh, "Motion control of protozoa for bio MEMS," *IEEE/ASME Trans. Mechatronics*, vol. 5, no. 2, pp. 181–188, June 2000.

[6] N. Ogawa, H. Oku, K. Hashimoto, and M. Ishikawa, "Microrobotic visual control of motile cells using high-speed tracking system," *IEEE Trans. Robotics*, vol. 21, no. 3, Jun. 2005 (to appear).

[7] ——, "Dynamics model of paramecium galvanotaxis for micro-robotic application," in *Proc. 2005 IEEE Int. Conf. Robotics and Automation (ICRA 2005)*, Apr. 2005, pp. 1258–1263.

[8] R. Thar, N. Blackburn, and M. Kühl, "A new system for three-dimensional tracking of motile microorganisms," *Applied and Environmental Microbiology*, vol. 66, no. 5, pp. 2238–2242, May 2000.

[9] J. R. Strickler, "Observing free-swimming copepods mating," *Philosophical Trans.: Biological Sciences, The Royal Society of London B*, vol. 353, pp. 671–680, 1998.

[10] S. C. Kuo and J. L. McGrath, "Steps and fluctuations of *Listeria monocytogenes* during actin-based motility," *Nature*, vol. 407, pp. 1026–1029, Oct. 2000.

[11] P. F. M. Teunis, F. Bretschneider, and H. Machemer, "Real-time three-dimensional tracking of fast-moving microscopic objects," *J. Microscopy*, vol. 168, no. 3, pp. 275–288, Dec. 1992.

[12] K. Hasegawa, A. Tanakadate, and H. Ishikawa, "A method for tracking the locomotion of an isolated microorganism in real time," *Physiology & Behavior*, vol. 42, no. 4, pp. 397–400, 1988.

[13] C. Zimmer, E. Labruyère, V. Meas-Yedid, N. Guillén, and J.-C. Olivo-Marin, "Segmentation and tracking of migrating cells in videomicroscopy with parametric active contours: A tool for cell-based drug testing," *IEEE Trans. Medical Imaging*, vol. 21, no. 10, pp. 1212–1221, 2002.

[14] S. T. Acton and N. Ray, "Detection and tracking of rolling leukocytes from intravital microscopy," in *Proc. 2004 IEEE Int. Symp. Biomedical Imaging (ISBI2004)*, Apr. 2004, pp. 1235–1238.

[15] H. C. Berg, "How to track bacteria," *Rev. Scientific Instruments*, vol. 42, no. 6, pp. 868–871, Jun. 1971.

[16] H. C. Berg and D. A. Brown, "Chemotaxis in *Escherichia coli* analysed by three-dimensional tracking," *Nature*, vol. 239, pp. 500–504, Oct. 1972.

[17] P. D. Frymier, R. M. Ford, H. C. Berg, and P. T. Cummings, "Three-dimensional tracking of motile bacteria near a solid planer surface," *Proc. National Academy of Sciences of the United States of America (PNAS)*, vol. 92, pp. 6195–6199, Jun. 1995.

[18] J. Enderlein, "Tracking of fluorescent molecules diffusing within membranes," *Applied Physics B: Lasers and Optics*, vol. 71, pp. 733–777, 2000.

[19] J. P. Armitage and H. L. Packer, "Bacterial motility and chemotaxis," in *Motion Analysis of Living Cells*, D. R. Soll and D. Wessels, Eds. Wiley-Liss, 1998, pp. 1–24.

[20] H. Oku, I. Ishii, and M. Ishikawa, "Tracking a protozoon using high-speed visual feedback," in *Proc. 1st Ann. Int. IEEE-EMBS Special Topic Conf. Microtechnologies in Medicine & Biology*, Oct. 2000, pp. 156–159.

[21] G. D. Hager, S. Hatchinson, and P. Corke, "A tutorial on visual servo control," in *Tutorial Note of 1996 IEEE Int. Conf. Robotics and Automation (ICRA'96)*, 1996.

[22] H. Toyoda, N. Mukohzaka, K. Nakamura, M. Takumi, S. Mizuno, and M. Ishikawa, "1ms column-parallel vision system coupled with an image intensifier; I-CPV," in *Proc. Symp. High Speed Photography and Photonics 2001*, vol. 5-1, 2001, pp. 89–92, (in Japanese).

[23] Y. Nakabo, M. Ishikawa, H. Toyoda, and S. Mizuno, "1ms column parallel vision system and its application of high speed target tracking," in *Proc. 2000 IEEE Int. Conf. Robotics & Automation (ICRA2000)*, Apr. 2000, pp. 650–655.

[24] M. Ishikawa, K. Ogawa, T. Komuro, and I. Ishii, "A CMOS vision chip with SIMD processing element array for 1 ms image processing," in *Dig. Tech. Papers of 1999 IEEE Int. Solid-State Circuit Conf. (ISSCC'99)*, 1999, pp. 206–207.

[25] I. Ishii, T. Komuro, and M. Ishikawa, "Method of moment calculation for a digital vision chip system," in *Proc. 5th IEEE Int. Workshop on Computer Architectures for Machine Perception (CAMP2000)*, Sept. 2000, pp. 41–48.

[26] W. T. Freeman, D. B. Anderson, P. A. Beardsley, C. N. Dodge, M. Roth, C. D. Weissman, W. S. Yerazunis, H. Kage, K. Kyuma, Y. Miyake, and K. Tanaka, "Computer vision for interactive computer graphics," *IEEE Computer Graphics and Applications*, vol. 18, no. 3, pp. 42–53, May/Jun. 1998.

[27] H. W. Smith and E. J. Davison, "Design of industrial regulators," in *Proc. IEE*, vol. 119, 1972, pp. 1210–1216.

[28] I. Ishii, Y. Nakabo, and M. Ishikawa, "Target tracking algorithm for 1ms visual feedback system using massively parallel processing," in *Proc. 1996 IEEE Int. Conf. Robotics & Automation (ICRA'96)*, vol. 3, Apr. 1996, pp. 2309–2314.

[29] H.-D. Görtz, Ed., *Paramecium*. Springer-Verlag, 1988.

[30] Y. Naitoh and K. Sugino, "Ciliary movement and its control in *Paramecium*," *J. Protozool.*, vol. 31, no. 1, pp. 31–40, 1984.

[31] A. Sakane, K. Hashigami, T. Tsuji, H. Ohtake, and M. Kaneko, "Model of taxis of paramecia based on the Hodgkin-Huxley equations," in *Proc. 2001 JSME Conference on Robotics and Mechatronics (Robomec'01)*, Jul. 2001 (in Japanese), pp. 2P2–B9.

[32] A. Hirano, M. Suzuki, T. Tsuji, N. Takiguchi, and H. Ohtake, "Mobile robot control based on chemotaxis of paramecia," in *Proc. 2004 JSME Conference on Robotics and Mechatronics (Robomec'04)*, Jun. 2004 (in Japanese), pp. 1A1–L1–23.

[33] H. S. Jennings, *Behavior of the Lower Organisms*. Columbia University Press, 1923.

[34] K. Ludloff, "Untersuchungen über den Galvanotropismus," *Archiv fur die Gesamte Physiologie*, vol. 59, pp. 525–554, 1895.

[35] T. Kamada, "Polar effect of electric current on the ciliary movements of Paramecium," *Journal of the Faculty of Science, Imperial University of Tokyo, Sect. IV, Zoology*, vol. 2, pp. 285–298, 1931.

[36] H. Oku, N. Ogawa, K. Hashimoto, and M. Ishikawa, "Two-dimensional tracking of a motile microorganism allowing high-resolution observation with various imaging techniques," *Rev. Scientific Instruments*, vol. 76, no. 3, Mar. 2005.

[37] N. Ogawa, H. Oku, K. Hashimoto, and M. Ishikawa, "Single-cell level continuous observation of microorganism galvanotaxis using high-speed vision," in *Proc. 2004 IEEE Int. Symp. Biomedical Imaging (ISBI 2004)*, Apr. 2004, pp. 1331–1334.